

# Design and Characterization of Model Linear Low-Density Polyethylenes (LLDPEs) by Multidetector Size Exclusion Chromatography

Sara V. Orski, Luke A. Kassekert, Wesley S. Farrell, Grace A. Kenlaw, Marc A. Hillmyer, and Kathryn L. Beers\*

Cite This: *Macromolecules* 2020, 53, 2344–2353

Read Online

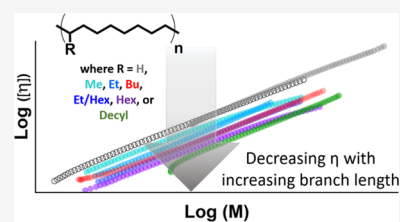
ACCESS |

Metrics & More

Article Recommendations

Supporting Information

**ABSTRACT:** Separations of commercial polyethylenes, which often involve mixtures and copolymers of linear, short-chain branched, and long-chain branched chains, can be very challenging to optimize as species with similar hydrodynamic sizes or solubility often coelute in various chromatographic methods. To better understand the effects of polymer structure on the dilute solution properties of polyolefins, a family of model linear low-density polyethylenes (LLDPEs) were synthesized by ring-opening metathesis polymerization (ROMP) of sterically hindered, alkyl-substituted cyclooctenes, followed by hydrogenation. Within this series, the alkyl branch frequency was fixed while systematically varying the short-chain branch length. These model materials were analyzed by ambient- and high-temperature size exclusion chromatography (HT-SEC) to determine their molar mass, intrinsic viscosity ( $[\eta]$ ), and degree of short-chain branching across their respective molar mass distributions. Short-chain branching is fixed across the molar mass distribution, based on the synthetic strategy used, and measured values agree with theoretical values for longer alkyl branches, as evident by HT-SEC. Deviation from theoretical values is observed for ethyl branched LLDPEs when calibrated using either  $\alpha$ -olefin copolymers (poly(ethylene-*stat*-1-octene)) or blends of polyethylene and polypropylene standards. A systematic decrease of intrinsic viscosity is observed with increasing branch length across the entire molar mass distribution. This work demonstrates the applicability of these model materials to deconvolute structure–property relationships using chromatographic separation techniques and is a step toward determining if sequence control can minimize compositional heterogeneity and generate improved standards for determining branching content in commercial polyolefins.



## INTRODUCTION

Due to the advancement of olefin polymerization catalysis, especially with the use of chain-shuttling catalysts, commercial production of polyolefins has expanded well beyond conventional linear or branched architectures. Now, well-controlled block copolymers and other polymer architectures can be produced on industrial scales, which expands polyolefin use as thermally stable thermoplastic elastomers.<sup>1–5</sup> However, a significant challenge that arises from using these expanded classes of polyolefins is the ability to separate and quantify, simultaneously, the molar mass, chemical composition, and architectural distributions within materials. Being able to accurately determine these key parameters is crucial for quantifying polyolefin structure–property–performance relationships.

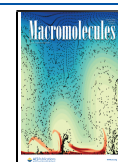
Separations of polyolefins have been achieved using fractionation techniques such as crystallization analysis fractionation (CRYSTAF),<sup>6</sup> crystallization elution fractionation (CEF),<sup>7</sup> and temperature rising elution fractionation (TREF),<sup>8</sup> which are all based on the fractional crystallinity or solubility of polymers, but often require very long times to fractionate and analyze the material. A more practical approach to characterize polyolefins is by the use of chromatographic

methods such as conventional high-temperature size exclusion chromatography (HT-SEC)<sup>9</sup> or high-performance liquid chromatography (HPLC).<sup>10,11</sup> More recently, advances in high-temperature liquid chromatography methods have utilized a discrete adsorption-promoting solvent barrier, introduced ahead of the polymer injection, to improve the effective separation of high-density polyethylene (HDPE) homopolymer chains from olefin block copolymers with similar enthalpic interactions.<sup>12</sup> Additionally, there has been limited work in multidimensional high-temperature chromatography (SEC  $\times$  HPLC) to separate polyolefins by molar mass and chemical composition, which includes hyphenated techniques to improve separation of polyolefins with non-crystallizable segments.<sup>13,14</sup>

Received: December 10, 2019

Revised: March 10, 2020

Published: March 27, 2020



Architectural distributions are an especially challenging type of heterogeneity to distinguish, as both long-chain branching (LCB) and short-chain branching (SCB) have impacts on the online detection methods conventionally used to characterize separations such as differential viscometry and light scattering.<sup>15,16</sup> Many advanced, commercial polyolefins contain both LCB and SCB architectures, which varies the bulk properties of the final product depending on their respective branching distributions. In LCB polyolefins, the branches are significantly longer than a few hydrocarbon units, which can have a considerable impact on polymer processing and rheology.<sup>17</sup> SCB polyolefins contribute to a reduction in bulk crystallinity, which affects the performance properties of the materials. Therefore, the ability to adequately quantify long-chain branching and short-chain branching distributions (LCBd and SCBd, respectively) in a polyolefin is important for quality control of the bulk material for commercial applications.

Empirical methods have been developed to “correct” for measured SCB content, using either offline NMR spectroscopy or online infrared (IR) detection to measure the methyl content as a function of total carbons ( $\text{CH}_3/1000$  total C) and then calculate the LCBd.<sup>16,18</sup> Recent work has also incorporated high-temperature quasi-elastic light scattering into HT-SEC to directly measure hydrodynamic radii in a quadruple detection SEC system and compare commercial polyolefins of different branching architectures.<sup>19</sup> For polyolefins that contain both SCB and LCB, standards are needed where the length of the SCB is known and the SCBd is constant across the molar mass distribution (MMD).  $\alpha$ -Olefin copolymers, where the SCB content is confirmed by offline methods such as NMR spectroscopy, currently fill this void. However, these techniques are limited in their ability to probe fundamental structure–property relationships given that the measured SCBd is an average of the SCB content at each given “slice” in a MMD curve; the resulting distribution is, in fact, a coelution of polyolefins with the same hydrodynamic volume, a phenomenon known as compositional dispersity.

With advances in controlled synthetic methods, such as ring-opening metathesis polymerization (ROMP), making model LCB and SCB polyolefins with improved control of functional group distribution along the polymer backbone is now possible. For example, ROMP of alkyl-substituted cycloolefins is a strategy to prepare polyalkenamers,<sup>20–31</sup> which upon hydrogenation can be transformed into linear low-density polyethylenes (LLDPEs). Cyclooctenes specifically have been employed to generate many functional polyoctenamers by ROMP, as the polymerization of cyclooctenes provides a balance of sufficiently high ring strain (31.0 kJ/mol, *cis*-cyclooctene and 69.9 kJ/mol, *trans*-cyclooctene) to achieve high yield polymerizations with straightforward preparation of the monomer feedstock and use of commercially available Grubbs catalysts.<sup>32</sup> The release of ring strain is the significant driving force that permits synthesis of controlled high molar mass polyoctenamers, based on conditions such as solvent, temperature, chain transfer agent concentration, catalyst loading, and monomer concentration. Sterically hindered cyclooctenes, such as 3-alkyl-*cis*-cyclooctenes and 1-alkyl-*trans*-cyclooctenes, can provide nearly ideal regio- and stereoregular polymers with functional groups incorporated at every eighth carbon along the polymer backbone.<sup>33–35</sup>

This presents an interesting opportunity for the use of hydrogenated poly(cyclooctene)s as model polyolefins to probe the differences in dilute solution properties using

multidetector SEC. As the short-chain branch structure and frequency are “programmed” into the repeat unit, these materials have limited potential for compositional dispersity upon separation. The strategy of using ROMP in designing these sequence-controlled SCB polymers also excludes the potential for LCB formation during polymerization. Furthermore, the flexibility of cyclooctene ROMP affords opportunities to modify the monomer structure and rapidly generate libraries of comparable LLDPEs to systematically study how changes to branching structure affect the final properties. Herein, we describe the synthesis of a family of well-controlled LLDPEs using ROMP of functionalized cyclooctenes to generate one branch point at exactly every eighth carbon along the chain. We analyzed this family of polyolefins by both high-temperature and ambient SEC to determine the impact of controlled chain architecture on dilute solution properties and observed a systematic decrease in intrinsic viscosity as a function of short-chain branch length.

## ■ EXPERIMENTAL SECTION

**Disclaimer.** Certain commercial equipment, instruments, or materials are identified in this paper to specify the experimental procedure adequately. Such identification is not intended to imply recommendation or endorsement by the National Institute of Standards & Technology, nor is it intended to imply that the materials or equipment identified are necessarily the best available for the purpose\*.

**General Procedures.** All air and moisture sensitive manipulations were carried out under an argon atmosphere using standard glovebox or Schlenk-line techniques. All NMR spectra were recorded on an Avance II 600 MHz or an Avance III 500 MHz Bruker spectrometer equipped with a broad-band inverse (BBI) room temperature probe and Sample Xpress automation system at room temperature in chloroform-*d* ( $\text{CDCl}_3$ ). All  $^1\text{H}$  chemical shifts are referenced to the residual solvent peak for  $\text{CDCl}_3$  (7.26 ppm). All  $^{13}\text{C}$  chemical shifts are referenced to  $\text{CDCl}_3$  (77.1 ppm).

**Materials.** *cis*-Cyclooctene (95%) was purchased from Alfa Aesar and passed through a plug of basic  $\text{Al}_2\text{O}_3$  prior to use. *Cis*-4-octene (97%), bromodecane (98%), magnesium turnings (>99%), and *p*-toluenesulfonyl hydrazide (98%) were purchased from Alfa Aesar and used without further purification. Grubbs second-generation catalyst, chlorodiphenylphosphine (96%), tributylamine (99%), Irganox 1010 (98%), hydrogen peroxide ( $\text{H}_2\text{O}_2$ ) solution (30 mass % in water), lithium ribbon (99.9% trace metal basis), sodium hydride (dry, 95%), anhydrous *N,N*-dimethylformamide (99.8%) (DMF), anhydrous diethyl ether ( $\geq 99.0\%$ ) ( $\text{Et}_2\text{O}$ ),  $\text{CDCl}_3$  (99.8 atom % D), *meta*-chloroperoxybenzoic acid ( $\leq 77\%$ ) (*m*-CPBA), *n*-pentane, and ethyl vinyl ether (99%) were purchased from Sigma-Aldrich and used without further purification. Glacial acetic acid (AcOH) was purchased from Mallinckrodt Chemical and used without further purification. The silica-supported platinum catalyst was obtained from Dow Chemical Company and used as received. Grubbs third-generation catalyst,  $(\text{H}_2\text{IMes})(3\text{-Br-pyr})_2(\text{Cl})_2\text{Ru}=\text{CHPh}$  (G3), was prepared according to literature procedures.<sup>36</sup> Dichloromethane (DCM) and tetrahydrofuran (THF) were distilled from  $\text{CaH}_2$  or Na, respectively, under argon prior to use in polymerizations. Other commercially available reagents were used without further purification.

**Synthesis of Model LLDPE. 1-Alkyl-*trans*-cyclooctenes.** The synthesis of *trans*-cyclooctene<sup>37</sup> and 1-butyl-*trans*-cyclooctene<sup>34</sup> and the polymers synthesized therefrom have been previously reported in the literature. 1-Decyl-*trans*-cyclooctene was prepared in a similar fashion to 1-butyl-*trans*-cyclooctene, as described below.

**1-Decyl-*cis*-cyclooctene.** Under the flow of argon, bromodecane (35.011 g, 0.158 mol) was added in portions to a stirring suspension of magnesium turnings (3.970 g, 0.163 mol) in 100 mL THF at 0 °C. The solution was then heated to 50 °C for 30 min under argon. After

cooling to room temperature, a solution of cyclooctenone (10.180 g, 0.081 mol) in 50 mL THF was added dropwise over the course of 30 min. The resulting solution was heated to 50 °C for 3 h. The solution was cooled to 0 °C and quenched by careful addition of saturated NH<sub>4</sub>Cl. The majority of the THF was removed in vacuo, and the aqueous solution was extracted with DCM. The combined organic layers were isolated and washed with saturated NaHCO<sub>3</sub>, followed by H<sub>2</sub>O, and then dried over Na<sub>2</sub>SO<sub>4</sub>. The solvent was removed in vacuo, and the crude product was transferred to a round-bottom flask equipped for vacuum distillation along with 3 drops of concentrated H<sub>2</sub>SO<sub>4</sub> and heated to 50 °C under reduced pressure (0.3 mmHg) for 2 h. At this point, <sup>1</sup>H NMR and IR spectroscopy revealed the presence of *n*-decane, *n*-icosane, 1-decene, and alcohol remaining in the flask. An additional 6 drops of concentrated H<sub>2</sub>SO<sub>4</sub> were added, and vacuum distillation was continued at 90 °C until no more distillate was collected. The product remaining in the flask was dissolved in hexane, washed with saturated NaHCO<sub>3</sub> and H<sub>2</sub>O, dried over Na<sub>2</sub>SO<sub>4</sub>, and concentrated to yield 1-decyl-*cis*-cyclooctene as a clear liquid (9.821 g, 49% yield). Despite long periods of vacuum distillation, a small amount of *n*-icosane is believed to remain as judged by NMR integration values. This impurity was removed by chromatography in a subsequent step (synthesis of 1-decyl-2-(diphenylphosphoryl)cyclooctanol). While this impurity does not interfere with reactivity in subsequent steps, its presence skews NMR integration values. <sup>1</sup>H NMR (600 MHz, CDCl<sub>3</sub>, 25 °C): δ 5.33 (t, *J* = 7.6 Hz, 1H), 2.14 (m, 2H), 2.09 (m, 2H), 1.97 (m, 2H), 1.57–1.44 (m, 9H), 1.44–1.22 (m, 24H), 0.89 (t, *J* = 7.2 Hz, 4H).

**1-Decyl-1,2-epoxycyclooctane.** 1-Decyl-*cis*-cyclooctene (9.821 g, 0.0392 mol) was dissolved in 20 mL DCM and added dropwise to a solution of *m*-CPBA (7.682 g, 0.0594 mol) in 130 mL DCM cooled to 0 °C. The solution was allowed to warm to room temperature and stirred for 1 h, at which point additional solid *m*-CPBA (2.195 g, 0.017 mol) was added and stirred overnight. After 16 h, an additional portion of solid *m*-CPBA (1.869 g, 0.014 mol) was added, and the solution was stirred for an additional 1 h. Saturated NaHCO<sub>3</sub> (100 mL) was added and stirred vigorously for 10 min. The organic layer was isolated and washed with 1 mol/L NaOH, followed by saturated NaHCO<sub>3</sub> and H<sub>2</sub>O. The organic layer was isolated and dried over Na<sub>2</sub>SO<sub>4</sub>, and the solvent was removed in vacuo to yield 1-decyl-1,2-epoxycyclooctane as a clear, viscous liquid (9.657 g, 92%). <sup>1</sup>H NMR (600 MHz, CDCl<sub>3</sub>, 25 °C): δ 2.68 (dd, *J* = 10.2, 4.5 Hz, 1H), 2.15 (m, 1H), 2.02 (dt, *J* = 13.6, 3.8 Hz, 1H), 1.89 (m, 1H), 1.68–1.17 (m, 34 H), 0.89 (t, *J* = 7.0 Hz, 4H).

**1-Decyl-2-(diphenylphosphoryl)cyclooctanol.** Chlorodiphenylphosphine (11.759 g, 0.053 mol) was added in portions over the course of 1 h to finely cut lithium ribbon (1.116 g, 0.161 mol) in 100 mL THF at room temperature under argon and stirred overnight. The resulting LiPPh<sub>2</sub> solution was decanted from the remaining lithium ribbon, and 1-decyl-1,2-epoxycyclooctane (9.658 g, 0.036 mol) was added dropwise at room temperature. The solution was heated to 50 °C under argon and stirred for 4 d. The resulting solution was then cooled to 0 °C, at which point AcOH (3.245 g, 0.054 mol) and H<sub>2</sub>O<sub>2</sub> (5.40 mL, 0.053 mol) were added dropwise, respectively. The solution was allowed to warm to room temperature and was stirred for 2 h, followed by addition of H<sub>2</sub>O (100 mL). The product was then extracted with DCM (3 × 100 mL). The combined organic layers were dried over Na<sub>2</sub>SO<sub>4</sub>, the solvent was removed in vacuo, and the product was purified by column chromatography on silica gel (100% ethyl acetate) to yield 1-decyl-2-(diphenylphosphoryl)cyclooctanol as a white, crystalline solid (13.563 g, 84% yield). <sup>1</sup>H NMR (600 MHz, CDCl<sub>3</sub>, 25 °C): δ 7.90 (m, 2H), 7.77 (m, 2H), 7.59–7.46 (m, 6H), 5.36 (d, *J* = 2.2 Hz), 3.26 (m, 1H), 1.95–1.64 (m, 7H), 1.60–1.43 (m, 6H), 1.42–1.00 (m, 22H), 0.90 (7, *J* = 7.1 Hz, 3H).

**1-Decyl-*trans*-cyclooctene.** Under argon, a suspension of NaH (1.001 g, 0.042 mol) in 40 mL anhydrous DMF was added dropwise to a solution of 1-decyl-2-(diphenylphosphoryl)cyclooctanol (13.563 g, 0.030 mol) in 120 mL anhydrous DMF at 0 °C. The reaction was allowed to warm to room temperature and was stirred vigorously for 2 h. The solution was cooled to 0 °C again, and 60 mL H<sub>2</sub>O was added carefully. After allowing to warm to room temperature again, the

solution was transferred to a separatory funnel, and the aqueous phase was extracted with *n*-pentane (150 mL). The organic layer was isolated and washed with saturated NaHCO<sub>3</sub> and H<sub>2</sub>O several times, then with saturated NH<sub>4</sub>Cl, and finally with concentrated NaOH and H<sub>2</sub>O to remove all phosphine byproducts. The organic layer was dried over Na<sub>2</sub>SO<sub>4</sub>, and the solvent was removed in vacuo, then redissolved in minimal DCM, filtered through a short pad of silica gel (100% DCM), and concentrated in vacuo again to yield monomer 3 as a clear liquid (4.866 g, 62% yield). <sup>1</sup>H NMR (600 MHz, CDCl<sub>3</sub>, 25 °C): 5.34 (dd, *J* = 12.7, 3.7 Hz, 1H), 2.38–2.25 (m, 3H), 2.13 (m, 1H), 1.99–1.80 (m, 5H), 1.68 (m, 1H), 1.62–1.38 (m, 4H), 1.36–1.23 (m, 15H), 0.94–0.87 (m, 4H), 0.64 (m, 1H). <sup>13</sup>C NMR (150 MHz, CDCl<sub>3</sub>, 25 °C): δ 142.4, 127.0, 39.6, 36.5, 33.8, 32.0, 31.3, 30.6, 30.1, 29.7, 29.7, 29.6, 29.5, 29.4, 29.4, 27.9, 22.7, 14.1 (Figures S1 and S2).

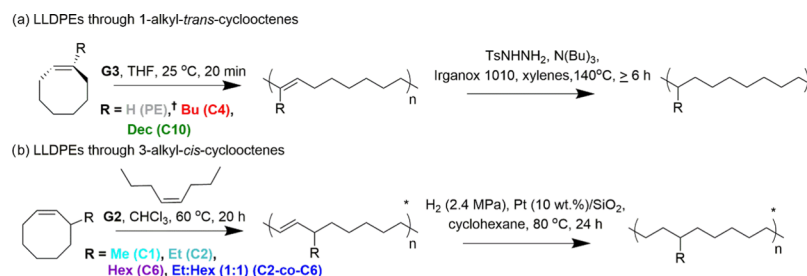
**Poly(1-decyl-*trans*-cyclooctene).** The polymerization and hydrogenation of 1-decyl-*trans*-cyclooctene follow the procedure previously reported for 1-butyl-*trans*-cyclooctene.<sup>34</sup> Poly(1-decyl-*trans*-cyclooctene): <sup>1</sup>H NMR (600 MHz, CDCl<sub>3</sub>, 25 °C): 5.10 (t, *J* = 7.5 Hz, 1H), 2.01–1.90 (m, 6H), 1.4–1.2 (m, 35H), 0.90 (t, *J* = 6.8 Hz, 5H). <sup>13</sup>C NMR (150 MHz, CDCl<sub>3</sub>, 25 °C): δ 139.59, 124.65, 37.02, 36.97, 31.96, 31.95, 30.25, 30.23, 30.07, 30.04, 29.86, 29.83, 29.73, 29.73, 29.71, 29.69, 29.68, 29.65, 29.64, 29.52, 29.43, 29.39, 29.38, 29.36, 28.56, 28.33, 27.28, 27.75, 22.72, 14.14, hydrogenated poly(1-decyl-*trans*-cyclooctene). <sup>1</sup>H NMR (600 MHz, CDCl<sub>3</sub>, 25 °C): 1.4–1.2 (m, 33H), 0.91 (t, *J* = 6.5 Hz, 3H). <sup>13</sup>C NMR (150 MHz, CDCl<sub>3</sub>, 25 °C): 37.46, 33.77, 31.96, 30.25, 30.20, 29.83, 29.76, 29.70, 29.40, 26.77, 26.72, 22.72, 14.14 δ (Figures S3–S6).

**3-Alkyl-*cis*-cyclooctenes.** Synthesis of the 3-alkyl-*cis*-cyclooctenes and corresponding homopolyalkenamers prepared therefrom has been previously reported in the literature,<sup>33</sup> and hydrogenation of these polymers was performed following known methods.<sup>38</sup>

**Poly(C2-*stat*-C6).** Anhydrous chloroform (28 mL), 3-ethyl-*cis*-cyclooctene (5.53 g, 40 mmol), 3-hexyl-*cis*-cyclooctene (7.77 g, 40 mmol), and *cis*-4-octene (31.4 μL, 0.202 mmol) were added to a flame-dried flask via syringe. The system was sparged with argon for 5 min while vigorously stirring and then immersed in an oil bath at 50 °C. G2 catalyst (17.0 mg, 0.020 mmol) was added as a solution in anhydrous, degassed CHCl<sub>3</sub> (0.3 mL) via a syringe. The reaction was cooled to room temperature after 20 h, quenched with ethyl vinyl ether (0.1 mL), stirred for an additional 15 min, and then cooled to 0 °C. The polymer was precipitated into methanol and decanted. The resulting polymer was dissolved in minimal DCM, and 10 mg of BHT was added. The solvent was removed in vacuo and further dried under high vacuum at 30 °C. The viscous, slightly yellow polymer (12.92 g, 97% yield) was then carried onto the next step. <sup>1</sup>H NMR (500 MHz, CDCl<sub>3</sub>, 25 °C): 5.35–5.25 (m, 2H), 5.11–5.03 (dd, *J* = 15.0, 8.5 Hz, 2H), 2.02–1.92 (m, 4H), 1.88–1.80 (m, 1H), 1.80–1.71 (m, 1H), 1.41–1.09 (m, 28H), 0.88 (t, *J* = 6.5 Hz, 3H), 0.82 (t, *J* = 7.5 Hz, 3H). <sup>13</sup>C NMR (125 MHz, CDCl<sub>3</sub>, 25 °C): δ 135.2, 134.8, 130.4, 130.1, 44.7, 42.92, 42.91, 35.74, 35.70, 35.3, 32.8, 32.7, 32.1, 29.91, 29.87, 29.6, 29.4, 28.3, 27.4, 27.2, 22.8, 14.2, 11.9 (Figures S7 and S8).

**Polyhydrogenated(C2-*stat*-C6).** Poly(C2-*stat*-C6) was hydrogenated using known methods<sup>38</sup> to give a transparent, viscous polymer (9.1 g, 91% yield). <sup>1</sup>H NMR (500 MHz, CDCl<sub>3</sub>, 25 °C): 1.34–1.14 (m), 0.89 (t, *J* = 7.0 Hz), 0.83 (t, *J* = 7.0 Hz). <sup>13</sup>C NMR (125 MHz, CDCl<sub>3</sub>, 25 °C): δ 39.0, 37.6, 33.86, 33.84, 33.4, 32.1, 30.3, 30.0, 29.9, 26.90, 26.86, 28.8, 26.0, 22.8, 14.2, 11.0 (Figures S9 and S10).

**High-Temperature Size Exclusion Chromatography (HT-SEC).** High-temperature size exclusion chromatography (HT-SEC) was performed using a Polymer Char GPC-IR instrument with an IR4 detector, a Wyatt Technology Dawn Heleos II multiangle light scattering detector (18 angles), and a four-capillary differential viscometer, as well as a Tosoh HT-EcoSEC instrument with differential refractive index (RI) detection. Samples were dissolved at concentrations between 1 and 2 mg/mL for 60 min at 135 °C with gentle agitation. Separations were conducted at 135 °C using 1,2,4-trichlorobenzene as the eluent, with 300 mg/kg Irganox 1010 added as antioxidant to the solvent reservoir. Five microliters of dodecane

Scheme 1. Synthetic Pathway for Model LLDPEs through (a) 1-Alkyl-*trans*-COEs and (b) 3-Alkyl-*cis*-COEs<sup>a</sup>

<sup>a</sup>The repeat unit has been shifted to highlight the branching that occurs at every eighth carbon along the polymer backbone for both synthetic pathways. <sup>†</sup>PE from *trans*-COE was catalyzed by G1/PPh<sub>3</sub>. The color coding for each of the LLDPEs here is continued throughout the manuscript.

**Table 1. Summary of the Number-Average Molar Mass, Dispersity ( $\mathcal{D}$ ), Short-Chain Branching, Mark–Houwink Parameter, and Conformation Plot Measurements Made by HT-SEC<sup>a</sup>**

sample	$M_n^b$ (kg/mol)	$\mathcal{D}^b$	SCB <sup>c</sup> (theoretical)	SCB <sup>c</sup> (LLDPE calibrated)	SCB <sup>c</sup> (PP/PE calibrated)	$\alpha^d$	$K$ (dL/g) $\times 10^{4d}$	$\nu^e$
linear PE	178 ± 8	1.5 ± 0.1	≈ 0	1.7 ± 0.1		0.70 ± 0.01	5.8 ± 0.6	0.59 ± 0.05
C1	37 ± 2	2.2 ± 0.2	111	79.6 ± 0.7	113.7 ± 1.0	0.62 ± 0.04	8.9 ± 0.5	0.52 ± 0.07
C2	32 ± 3	1.8 ± 0.1	100	85.4 ± 0.8	122.0 ± 1.1	0.72 ± 0.03	3.9 ± 0.8	
C4 <sup>f</sup>	29 ± 3	3.1 ± 0.3	83	83.4 ± 1.5	116.7 ± 1.9	0.67 ± 0.04	7.2 ± 6.0	0.61 ± 0.03
	121 ± 5	1.1 ± 0.1						0.60 ± 0.04
	235 ± 1	2.1 ± 0.1						0.42 ± 0.03
C2-co-C6	40 ± 3	1.9 ± 0.1	86	76.4 ± 1.0	109.1 ± 1.5	0.71 ± 0.03	2.6 ± 0.2	
C6	39 ± 4	2.1 ± 0.2	71	70.1 ± 0.9	100.0 ± 0.9	0.69 ± 0.03	4.2 ± 1.3	0.47 ± 0.06
C10 <sup>f</sup>	92 ± 3	1.6 ± 0.1	56	54.3 ± 2.3	78.0 ± 2.8	0.73 ± 0.02	2.1 ± 0.7	0.64 ± 0.01
	314 ± 5	1.8 ± 0.0						0.53 ± 0.08

<sup>a</sup>All reported error in measurements represents one standard deviation of the data among repeat injections. <sup>b</sup>Reported molecular masses and molecular mass distributions calculated from MALS detection. <sup>c</sup>Degree of short-chain branching (SCB): theoretical values were calculated based on CH<sub>3</sub>/1000 total C; LLDPE calibrated and PP/PE calibrated values were determined using IR detection. <sup>d</sup>Mark–Houwink parameters measured by HT-SEC: slope ( $\alpha$ ) and intercept ( $K$ ). <sup>e</sup>Slope of RMS conformation plot ( $\log R_g$  vs  $\log(M)$ ). C2 and C2-co-C6 were not included because the lower molar mass range caused significant noise in calculating accurate  $\nu$  above the MALS limit of detection of  $R_g \geq 10$  nm. <sup>f</sup>Varying molar masses for C4 and C10 were prepared. Theoretical and measured SCB and Mark–Houwink parameters reflect the average values of the respective molar mass series.

was added to each vial as a flow rate marker. The stationary phase for both systems was a set of 3 Tosoh HT columns (2 Tosoh TSKgel GMH<sub>HR</sub>-H (S) HT2, 13  $\mu$ m mixed bed, 7.8 mm ID  $\times$  30 cm columns and 1 Tosoh TSKgel GMH<sub>HR</sub>-H (20) HT2, 20  $\mu$ m, 7.8 mm ID  $\times$  30 cm column with an exclusion limit  $\approx 4 \times 10^8$  g/mol). For the Tosoh instrument, narrow dispersity polyethylene standards were used for calibration. For the Polymer Char instrument, narrow dispersity polystyrene standards were used for column calibration. NIST SRM 1475a (linear, broad, HDPE) was used as a linear standard for the viscometer and multiangle light scattering (MALS) detector and to calibrate the voltage response of each. NIST SRM 1478 was used to calibrate the interdetector delay and normalize the photodiode response of the MALS detector. Composition standards consisting of 6,  $\alpha$ -olefin copolymer LLDPE standards (poly(ethylene-*stat*-1-octene), 2.6–45.3 CH<sub>3</sub>/1000 total C) from Polymer Char were used to calibrate the IR response from the methyl and alkyl absorption bands. A second calibration curve to calibrate the IR was constructed out of blends of polyethylene (PE) and polypropylene (PP), where the total areas of the IR responses were plotted against the average SCB content, which was confirmed offline by NMR. Calibration and data analyses were performed with proprietary software from each instrument vendor. Data processing for the HT-SEC data was conducted using a linear Zimm<sup>39</sup> formalism to fit the light scattering data for molar mass determinations, and the  $dn/dc$  for all HT-SEC data was fixed at  $-0.104$  mL/g. The uncertainty in the molar masses obtained by this measurement is  $\pm 1.5\%$ . All injections were done at least three times, and the reported error on all measurements is one standard deviation of the mean. RMS conformation plots ( $\log R_g$  vs  $\log M$ ) were calculated from light scattering data using Berry<sup>40</sup> formalism with a third-order fit to

compare the radii of gyration ( $R_g$ ) across the large range of molar masses for the polymers in this study with a high degree of linearity.<sup>40,41</sup> Angles 2 (28°) and 18 (147°) were excluded from the fit to ensure excess noise did not overly skew the fitting between repeat injections.

**Ambient-Temperature Size Exclusion Chromatography (SEC).** SEC measurements were conducted on a Tosoh EcoSEC system with differential refractive index (RI) detection coupled to a Wyatt Dawn Heleos II multiangle light scattering detector (18 angles) and a Wyatt Viscostar III differential viscometer. The separation used THF as the eluent at 35 °C, and the stationary phase was a set of two Tosoh mixed pore columns (2  $\times$  TSKgel GMH<sub>HR</sub>-H). Data were collected using Astra 7, and molar masses were determined based on light scattering data fit to a linear Zimm formalism.<sup>39</sup> The differential refractive index increment ( $dn/dc$ ) values used for each polymer were measured from offline batch injections.

**Vibrational Spectroscopy.** Infrared (IR) spectra were recorded on a Thermo Scientific Nicolet 6700 FTIR instrument with a ZnSe attenuated total reflection (ATR) single-bounce crystal at 60°, with a spectral resolution of 2  $\text{cm}^{-1}$  and 128 scans per spectrum using a deuterated triglycine sulfate (DTGS) detector. Samples on the ATR crystal were put in immediate contact by compression with a freshly cleaned gold-coated silicon wafer, which is IR reflective. Solution IR of the LLDPEs was taken using a PTFE IR card, and solutions of LLDPEs in 1,2,4-trichlorobenzene (5 mg/mL) were measured in transmission mode and a liquid-nitrogen-cooled MCT (mercury cadmium telluride) detector at a resolution of 4  $\text{cm}^{-1}$  and 128 scans per spectrum.

## RESULTS AND DISCUSSION

**Synthetic Design of LLDPEs.** To determine the influence of controlled chain architecture on the dilute solution properties of polyolefins, a family of LLDPEs were synthesized using the ROMP of both 1-alkyl-*trans*-cyclooctenes and 3-alkyl-*cis*-cyclooctenes to generate regioregular polyalkenemers, which were subsequently hydrogenated to the corresponding regioregular LLDPEs.<sup>33,34</sup> As these alkyl-substituted polyolefins are all based on sterically hindered cyclooctenes, we expect that the polymerizations of each monomer will yield very high degrees of head-to-tail addition (>95%), as has been reported in previous studies.<sup>33,34</sup> Propagation of the monomers in this manner will result in the spacing between branch points on the LLDPEs to be eight carbons long, regardless of which monomer is used. This means that differences in the dilute solution characteristics of the 1-*trans*-cyclooctenes versus the 3-*cis*-cyclooctenes by SEC should originate exclusively from the differences in the short-chain branch lengths. A summary of the reaction schemes for the family of LLDPEs, as well as the polymerization of *cis*-cyclooctene for a comparative PE, is shown in Scheme 1. The structural details of the LLDPE series can be found in Table 1. The polymers are labeled according to their representative branching substitutions. For example, the butyl-substituted polyethylene sample is labeled as C4 to indicate that the branch is a four-carbon chain. The PE control does not contain any substitutions and therefore has no degree of branching.

As the branch frequency is built into the monomer repeat unit, the theoretical SCB content of each polymer was calculated (Table 1). The molar masses and dispersities are representative of the main molar mass distribution; however, some oligomeric species are present in the 3-alkyl-*cis*-cyclooctene concentration detector data from HT-SEC characterization (RI and IR detection), which may include cyclic oligomers, as a result of intramolecular chain transfer, or backbiting, as has been reported in the literature.<sup>33</sup> Representative raw chromatograms showing RI, IR, specific viscosity, and 90° light scattering for the HT-SEC data are available in Figures S11–S16 of the Supporting Information.

**Determination of Short-Chain Branching Distributions of LLDPEs via HT-SEC with IR Detection.** To determine the SCBd of the polymer series, high-temperature size exclusion chromatography with infrared detection (HT-SEC-IR) was used. Infrared spectroscopy allows us to determine the CH<sub>3</sub>/1000 total carbon ratio (SCB content) of the polymers in the LLDPE family by observing the contributing IR intensities of the methyl and alkyl vibrational modes. Coupling this type of detection to SEC results gives us a direct measurement of polymer SCBd. Representative MMDs and SCB content of the LLDPEs characterized by HT-SEC-IR are found in Figure 1. On comparing with the results obtained from the average SCB content by HT-SEC-IR (Table 1), an agreement between experimental and theoretical SCB contents is observed for the linear PE, C4, C6, and C10 LLDPEs with very little variation between trials. The SCB content is constant across the MMD, with variability only at the very ends of the integration limits where detector noise is a contributing factor. The overall areas of the methyl and alkyl IR responses for those fractions of the elution curve are very small relative to the baseline; this would lead to additional error in the SCB content at those molar mass fractions. Even so, the variability observed across the MMD in Figure 1 is

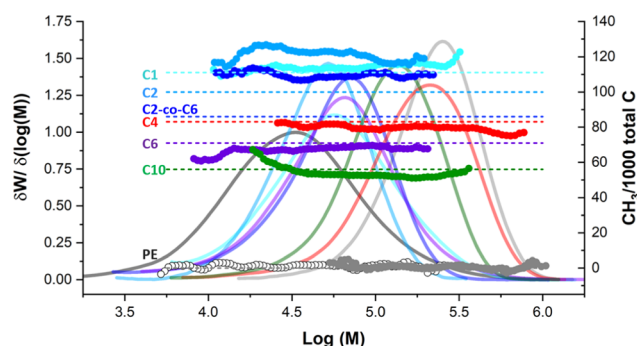


**Figure 1.** Molar mass distribution of model LLDPEs (left axis, solid line) in this study. Short-chain branching content (SCB, CH<sub>3</sub>/1000 total C, right axis, solid dots) was calibrated against  $\alpha$ -olefin copolymer standards (C4, C6, and C10) or PP/PE blends (C1, C2, and C2-co-C6) as a calibration curve. Linear PE synthesized from *trans*-cyclooctene (light gray, filled gray symbol) and a linear PE standard (NIST 1475, dark gray, open symbol) are included for comparison. Theoretical SCB content for each LLDPE is indicated by the dashed line.

below the stated measurement resolution of the IR4 detector at  $\leq 10$  CH<sub>3</sub>/1000 total C. The disagreement between theoretical and measured SCB for C1, C2-co-C6, and C2 for each polymer studied was unexpected as the branching content is built into the monomer repeat unit and the ROMP mechanism utilized should not result in deviations in the methyl content. Differences in calibration curves for flow-through IR detection in  $\alpha$ -olefin copolymers of different branch lengths have been documented in the literature.<sup>42,43</sup> Subtle differences in the absorbance maxima of the different branched polyolefins and their overlap with the narrow methyl IR filter, as well as the broad-band alkyl filter, can result in different calibration curves. We verified the differences previously reported in the literature<sup>42</sup> by constructing both a calibration curve that uses commercially available  $\alpha$ -olefin copolymers of known methyl content and blends of PE and PP from 100% PE to 100% PP (333 CH<sub>3</sub>/1000 total C), shown in Figure S17 of the Supporting Information.

The two different types of calibrants result in distinct calibration equations. The calibration curves for the LLDPE ( $\alpha$ -olefin copolymer) and blends of PP/PE have linear fits, described by the following equations

$$A_{\text{CH}_3/\text{alkyl}(\alpha\text{-olefin copolymer})} = 2.59 \times 10^{-3} [\text{CH}_3/1000 \text{ total C}] + 0.63$$

$$(R^2 = 0.9999)$$

$$A_{\text{CH}_3/\text{alkyl}(\text{PP-PE blend})} = 1.78 \times 10^{-3} [\text{CH}_3/1000 \text{ total C}] + 0.63$$

$$(R^2 = 0.9990)$$

While the previous report<sup>42</sup> cites a quadratic model dependence for the IR detector when C1 polymers are measured, we do not observe a statistically significant improvement in fit quality in using a polynomial fit over a linear one for our IR detector. Using the PP/PE blends improves the accuracy of the C1 LLDPE measured values to  $113.7 \pm 1$  CH<sub>3</sub>/1000 total C, which is very close to the theoretical values of 111 CH<sub>3</sub>/1000 total C, shown in the light blue dashed line in Figure 1. The PE/PP calibration curve overestimates the C2-containing LLDPEs (C2 and C2-co-C6), while the  $\alpha$ -olefin calibration curve underestimates them significantly (see Table 1). To investigate this discrepancy,

full Fourier transform infrared spectroscopy (FTIR) data of the alkyl region was measured using attenuated total reflection (ATR)-FTIR in the bulk state (Figure 2), as well as in solution

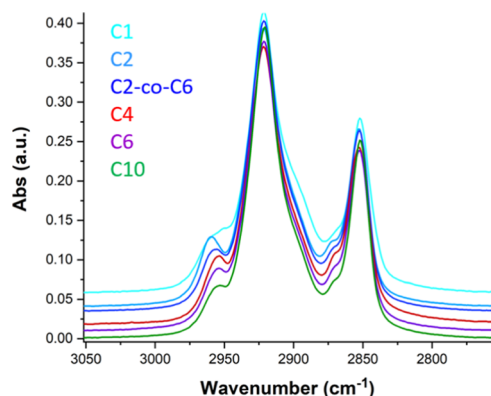


**Figure 2.** ATR-FTIR measurements of model LLDPEs in this study across the alkyl CH stretching region relevant to HT-SEC with IR detection. The total area of the alkyl region (2800–3000  $\text{cm}^{-1}$ ) has been normalized between the spectra for comparison. Note the shift in the methyl asymmetric stretch centered near 2950  $\text{cm}^{-1}$  for each branch length.

(Figure S18). The spectral information of the flow-through IR filters on the HT-SEC instrument is unavailable as it is the intellectual property of the manufacturer and was not disclosed to us.<sup>43</sup> The IR4 detector contains one narrow filter for the asymmetric methyl stretch located at  $\nu_{\text{CH}_3} \approx 2950 \text{ cm}^{-1}$  and one broad-band filter covering the entire alkyl CH stretching region from  $\nu_{\text{alkyl}} = 2800$  to  $3000 \text{ cm}^{-1}$ . ATR-FTIR peak maxima for the C4, C6, and C10 methyl asymmetric stretches were all located at  $\nu_{\text{C4}} = \nu_{\text{C6}} = \nu_{\text{C10}} = 2953 \text{ cm}^{-1}$ . A distinct shift is observed, however, for the C2-containing polymers for the methyl asymmetric stretch, as  $\nu_{\text{C2}} = 2960 \text{ cm}^{-1}$  and  $\nu_{\text{C2-co-C6}} = 2957 \text{ cm}^{-1}$ . This general trend is also consistent in the solution FTIR measurements and with the observations in the HT-SEC-IR data. If the methyl filter for the IR detector is sufficiently narrow to exclude significant portions of the higher wavenumbers from the included absorbance measured, this would account for the underestimation of the C2 and C2-co-C6 LLDPE SCB contents when using the  $\alpha$ -olefin calibration curve. The high SCB content, greater than 70  $\text{CH}_3/1000$  total C, has been reported to be an approximate limit to the linear calibration of the SCB with a single  $\alpha$ -olefin copolymer as blends of different  $\alpha$ -olefins showed different quadratic curves in their previous study.<sup>43</sup> However, we observe good agreement between theoretical branching content between the C4, C6, and C10 and those measured using the  $\alpha$ -olefin calibration curve. While further study would have to be done to evaluate its efficacy, the use of well-controlled branched polyolefin copolymers may extend the linearity of IR calibrations and provide more dynamic calibration ranges for highly SCB materials.

#### Dilute Solution Viscosity Studies of LLDPE Series.

Dilute solution viscosity measurements of the LLDPE and PE were measured using an online viscometer to generate Mark–Houwink plots, which relate the change in intrinsic viscosity ( $[\eta]$ ) of the polymer to its molar mass across the MMD (Figure 3) and are defined by the relationship,  $[\eta] = KM^\alpha$ , where  $M$  is the molar mass, and  $K$  and  $\alpha$  are the empirically determined constants. These constants can be determined by

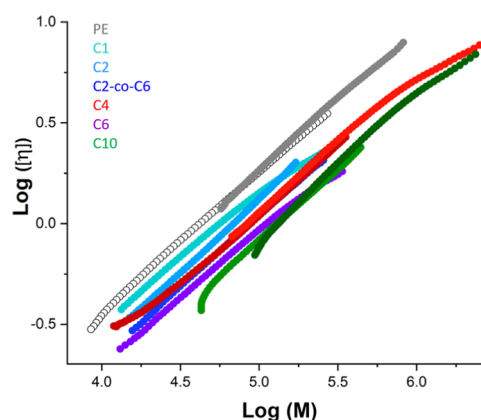


**Figure 3.** Mark–Houwink plots of LLDPEs measured by HT-SEC. The open circles are the intrinsic viscosity data measured for NIST SRM 1475A, for reference.

plotting the  $\log([\eta])$  versus  $\log(M)$ , which produces a linear trend where the Mark–Houwink slope is  $\alpha$  and the intercept is  $\log(K)$ . The values for  $\alpha$  and  $K$  are shown in Table 1 for all samples measured by HT-SEC. The PE synthesized from *trans*-cyclooctene agrees well with NIST 1475A, a linear PE standard, as the intrinsic viscosity plot of the standard and the PE overlay across the entire MMD. A systematic decrease in intrinsic viscosity is observed with increasing SCB length and is consistent across the molar mass distribution overall. Furthermore, the slope of the Mark–Houwink plot is consistent across all samples, as shown in the  $\alpha$  values in Table 1, where the average of all slopes  $\alpha_{\text{avg}} = 0.69 \pm 0.04$ . Previous work on the investigation of  $\alpha$ -olefin statistical copolymers shows a systematic decrease in intrinsic viscosity with increasing SCB copolymer content, as the higher SCB frequency would result in a smaller hydrodynamic size at the same molar mass.<sup>15</sup> The LLDPEs analyzed here demonstrate that intrinsic viscosity also decreases with longer SCB length at a fixed branching frequency for polymers of comparable molar mass.

Slight deviations from linearity are observed in the Mark–Houwink plots at the high end of the MMD, particularly in high molar mass C4 and C10 LLDPE samples, as well as in the C1 and C6 samples, which is potentially indicative of branch formation. The C4 and C10 polyalkenamers (prehydrogenated material) were also analyzed by HT-SEC-IR and showed no significant deviation in the Mark–Houwink plot. These curves are shown in Figure S19 of the Supporting Information. To investigate this further, the Mark–Houwink plot for the LLDPEs was compared to the conformation plot (Figure S20 of the Supporting Information), relating the radius of gyration ( $R_g$ ) to molar mass by the power law:  $R_g = KM^\nu$ , where the exponent,  $\nu$ , is the scaling factor, with  $\nu \approx 0.588$  representing the Flory exponent for linear chains.<sup>44</sup> An upturn in the conformation plots of the high molar mass C4 and C10 LLDPEs is indicative of anchoring, which is a non-size-exclusion-based separation of high molar mass and, often, LCB polymer chains being retained in the stationary phase pores and eluting later in the chromatogram. In addition, the smaller slopes of the conformation plot for the high molar mass C4 and C10 relative to their lower molar mass counterparts suggest a random branching structure, as  $\nu_{\text{C4-H}} = 0.42 \pm 0.03$  and  $\nu_{\text{C10-H}} = 0.53 \pm 0.08$ , while  $\nu_{\text{C4}} = 0.61 \pm 0.03$  and  $\nu_{\text{C10}} = 0.64 \pm 0.01$  (Table 1), respectively. Based on the conformation

and Mark–Houwink plots, we are confident that the high molar mass C4 and C10 polymers contain LCB. We conclude that the source of the apparent LCB in the C4 and C10 high molar mass polymers is interchain cross-linking during the hydrogenation process. Despite the addition of excess antioxidant, this coupling of chains occurs as it takes several hours of refluxing in xylenes to achieve quantitative conversion of the polyalkenamer by  $^1\text{H}$  NMR spectroscopy.<sup>34</sup> While these cross-links do not result from the original polymerization, the low level of chain coupling results in macromolecules that retain solubility and impact the viscosity data, looking effectively like LCB. By applying a power law to the linear and “branched” portion of the Mark–Houwink plots, we can calculate the average molar mass between LCB segments ( $M_{\text{seg}}$ ) for each polymer from the intersection of the two lines<sup>45,46</sup> as  $M_{\text{seg,C}_4} = (481 \pm 71)$  kg/mol and  $M_{\text{seg,C}_{10}} = (516 \pm 54)$  kg/mol. Calculations of similar crossover points using the conformation plot data  $M_{\text{seg,C}_4} = (414 \pm 46)$  kg/mol and  $M_{\text{seg,C}_{10}} = (509 \pm 62)$  kg/mol were done. The consistency between viscosity and light scattering data leads us to believe that the calculations of  $M_{\text{seg}}$  have merit, although it should be noted that the presence of anchoring indicates coelution of branched molecules at low molar mass, which may affect the conformation plot slope in that region and calculation of the crossover point for  $M_{\text{seg}}$ .

The C1 and C6 confirmation plots do not demonstrate anchoring phenomena; however, the low molar mass upswing of the conformation plot is negligible in the case of polymers with a lower degree of branching, branched samples that do not contain molecules with very high molar masses, or polymers with relatively short branches.<sup>47</sup> We cannot confirm the presence of LCB in C1 and C6 samples by MALS measurement of  $M_{\text{seg}}$ , as the conformation plots are slightly shifted above the conformation plot for the linear PE. Qualitatively, the downturn of the Mark–Houwink plots suggests small amounts of random chain branching in C1 and C6 as we do see a lower slope in the conformation plot of the C1 and C6 relative to their lower molar mass counterparts, shown in Table 1, which is indicative of random branching of the polymer chain.

The viscometric contraction factor  $g'$  was calculated to highlight the systematic decrease in viscosity relative to the linear PE (Figure 4) across the molar mass distribution. The contraction factor is the ratio of the intrinsic viscosity of a

branched polymer to the intrinsic viscosity of a linear polymer of the same molar mass. For lower molar masses, a decrease in  $g'$  is observed for C1, C2, C2-co-C6 and C4, C6, and C10 of approximately 0.1 with each increasing SCB LLDPE. The magnitude of the apparent viscosity change is dependent on a number of factors, including the differential refractive index increment ( $dn/dc$ ) and the second virial coefficient ( $A_2$ ), among others. These experimental differences can be compared to theoretical molecular dynamics simulations to investigate the degree to which experimental intrinsic viscosity values agree with theoretical predictions.

$$g' = \left( \frac{[\eta]_{\text{B}}}{[\eta]_{\text{L}}} \right)_M$$

Generally, MALS determination of branching is considered more accurate than viscometric calculations, because the viscosity shielding ratio ( $\epsilon$ ) must be known and assumed to be constant across the MMD to convert the contraction factor ( $g$ , from the ratio of the mean square radius of the branched polymer to its linear analogue) to  $g'$ . The type of branching must also be known to determine the branching number as well as the branching frequency.<sup>48,49</sup> These calculations were not performed on these data, however, due to *a priori* knowledge required regarding branching topology. It is difficult to quantify whether LCB is trifunctional (3 arms per branch site) or tetrafunctional (4 arms per branch site) for PE branching induced by radical mechanisms.<sup>49</sup>

As shown in the overlay of the conformation plots (Figure S20), while the slopes are indicative of a well-solvated, random coil, there is no decrease in  $R_g$  with increase in SCB length as is observed in the Mark–Houwink plots. We attribute this to the specific refractive index increment of PE being used for all samples analyzed, as the intensity of scattered light scales with  $(dn/dc)^2$ . Error in  $dn/dc$  would have a significant impact on the molar mass determination and shift the  $x$ -axis ( $\log M$ ) on the resulting conformation plot. Previous studies of PE-LLDPE copolymers have demonstrated that increasing SCB content can change  $dn/dc$  values by as much as a 10%.<sup>15</sup> Direct measurements of batch  $dn/dc$  for the LLDPEs at high temperature are not currently feasible in our laboratory, and calculations of  $dn/dc$  by assuming 100% mass recovery were not highly reproducible.

The high degree of SCB in the LLDPEs of moderate molar masses yields amorphous polymers, which have improved solubility in organic solvents relative to conventional LLDPEs. Comparative analysis was therefore conducted in an ambient SEC system with THF as the eluent at 35 °C, summarized in Table 2 and Figures S11–S16 of the Supporting Information. The molar masses determined for the C1–C10 polymers are comparable with HT-SEC results (Table 1). A summary of the Mark–Houwink plots for the analysis is shown in Figure 5; similar to the HT-SEC data, there is a decrease in intrinsic viscosity with increasing branch length. It is interesting that C10 shows a slight upturn in the Mark–Houwink plot at high molar masses, while a slight downturn is noted for the other LLDPEs (e.g.,  $\alpha_{\text{C}_2\text{-co-C}_6} \approx 0.58\text{--}0.52$ ), indicative of a more compact structure.<sup>19,50</sup> The slope of the Mark–Houwink plots overall is close to 0.5, signifying near- $\theta$  conditions in THF at 35 °C. The longer SCB structure of the C10, as well as the regular spacing of the SCB, may result in a stiffer chain at high molar masses. The rise in slope with increasing molar mass from the initially  $\alpha_{\text{C}_{10}} \approx 0.46$  to 0.61 indicates a structural

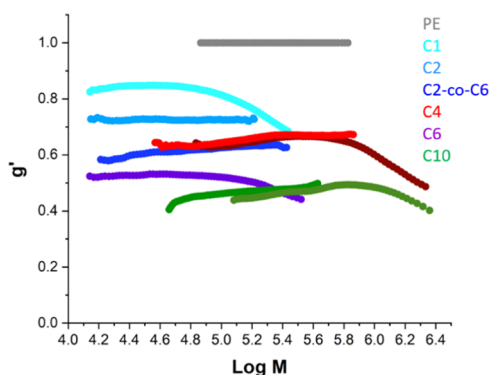


**Figure 4.** Viscometric contraction factor,  $g'$ , across the molar mass distribution for the model LLDPEs studied.  $g' = 1$  for linear polyethylene.

Table 2. Summary of Molar Mass, Dispersity ( $\bar{D}$ ), and Mark–Houwink Parameter Measurements Made by SEC (THF, 35 °C)<sup>a</sup>

sample	$M_n^b$ (kg/mol)	$\bar{D}^b$	$dn/dc^c$ (mL/g)	$\alpha^d$	$K$ (dL/g) $\times 10^4{}^d$	$\nu^e$
C1	49 $\pm$ 2	1.9 $\pm$ 0.1	0.076	0.55 $\pm$ 0.03	19 $\pm$ 7.4	0.48 $\pm$ 0.02
C2	38 $\pm$ 2	1.6 $\pm$ 0.1	0.080	0.61 $\pm$ 0.06	8.9 $\pm$ 5.6	0.62 $\pm$ 0.10
C4	47 $\pm$ 2	2.1 $\pm$ 0.3	0.079	0.68 $\pm$ 0.03	3.2 $\pm$ 0.9	0.46 $\pm$ 0.11
C2-co-C6	38 $\pm$ 3	1.9 $\pm$ 0.0	0.079	0.61 $\pm$ 0.03	7.4 $\pm$ 3.0	0.57 $\pm$ 0.07
C6	37 $\pm$ 1	2.2 $\pm$ 0.1	0.079	0.58 $\pm$ 0.05	9.2 $\pm$ 4.8	0.49 $\pm$ 0.05
C10	88 $\pm$ 0	1.6 $\pm$ 0.1	0.084	0.64 $\pm$ 0.06	4.7 $\pm$ 3.2	0.59 $\pm$ 0.02

<sup>a</sup>All reported error in measurements represents one standard deviation of the data among repeat injections. <sup>b</sup>Reported molecular masses and dispersities are from values calculated from MALS detection. <sup>c</sup>Differential refractive index increments ( $dn/dc$ ) were determined using offline batch injections. <sup>d</sup>Mark–Houwink parameters measured by HT-SEC: slope ( $\alpha$ ) and intercept ( $K$ ). <sup>e</sup>Slope of RMS conformation plot ( $\log R_g$  vs  $\log(M)$ ).

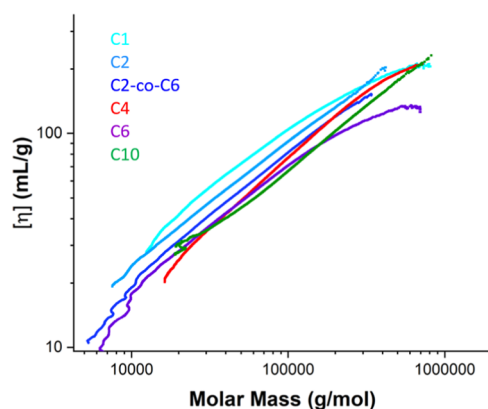


Figure 5. Mark–Houwink plot of LLDPEs measured by SEC (THF, 35 °C).

conversion from a primarily linear coil in a  $\theta$ -solvent to a more rigid conformation. This upturn in the Mark–Houwink plot has also been reported in recent work by Dockhorn et al. for high molar mass bottlebrush-type polyethylene structures synthesized by chain-walking catalysts.<sup>50</sup> The change in the  $R_g$  scaling with molar mass,  $\nu$ , does not change significantly across the MMD for the ambient SEC data. As a qualitative comparison, the slope changed for C1 and C6 from the low- to high molar mass regions of the ambient Mark–Houwink plots from  $\alpha_{C1} \approx 0.61$  to 0.29 and from  $\alpha_{C6} \approx 0.59$  to 0.22, respectively. This larger change in  $\alpha_{C1}$  and  $\alpha_{C6}$  indicates a structural conversion from a primarily linear coil to a more compact topology at higher molar masses. Most likely, an increase in LCB mainly contributes to this change, as also supported by similar changes in the HT-SEC viscometry and conformation plots for those polymers (see Figures 3 and S20 of the Supporting Information).

The viscometric contraction factor could not be determined for these samples, however, as the insolubility of PE in THF prevented the measurement of the comparable linear analogue. Representative conformation plots for the ambient SEC-MALS are shown in Figure S21 of the Supporting Information. The resultant slopes of the conformation plot are  $\nu = 0.53 \pm 0.07$  overall. The change in the slope of the conformation plot in Figure S21 between lower and higher molar masses is very slight and follows the trends observed in the viscosity data, where there is a slight downturn in RMS radii at high molar mass and a slight upturn for the C10 LLDPE, as evidenced by the  $\nu_{C10, \text{avg}}$  in Table 2 of  $0.59 \pm 0.02$ .

In comparing the high-temperature and ambient data, molar mass calculations are consistent between both analyses and the trends in Mark–Houwink plots and conformation plots are similar. While the solvent conditions for LLDPE analysis in

THF are near- $\theta$  conditions, the overall  $\alpha$  scaling between Mark–Houwink plots indicates that the polymers are in good solvent, as the approximated fractal dimension,  $d_f$ , indicates a linear random coil in a good solvent ( $1.67 \leq d_f \leq 2$ ), as  $d_{f\{\text{TCB}, 135\text{ °C}\}} = 1.77 \pm 0.08$  and  $d_{f\{\text{THF}, 35\text{ °C}\}} = 1.86 \pm 0.05$ . Both conformation plots for the HT and ambient data show that the low molar mass C10 LLDPE has a slightly larger slope than the rest of the series, which suggests a more rigid structure with the longer SCB length.

$$d_f = \frac{3}{\alpha + 1}$$

In future studies, measurements of  $A_2$  through static light scattering or small-angle neutron scattering would be useful in differentiating topological phenomena versus conformation effects for different LLDPEs under different solvent conditions. Measurements to evaluate the degree of compactness would need to be investigated through C1, C2, and C2-co-C6 polymer families across a range of molar masses. Addition of online quasi-elastic light scattering would aid in the interpretation of topological and conformation changes with molar mass, as the ability to quantify the hydrodynamic radius ( $R_h$ ) as a function of molar mass enables the determination of dimensionless radii ratios, such as  $\rho = R_h/R_g$ .<sup>19</sup> In addition, evaluation of  $\kappa = R_\eta/R_g$ <sup>19,51</sup> can be useful for assessing changes in compactness and would be beneficial in future studies where a molar mass series is compared for a single LLDPE and the  $dn/dc$  at high temperature are measured directly.

## CONCLUSIONS

A family of LLDPEs were synthesized from alkyl-functionalized cyclooctenes with SCB lengths between 1 and 10 carbons. The SCB distributions are constant across the MMD and agree with theoretical values with the exception of the ethyl-containing LLDPEs, which is attributed to the shift in the methyl asymmetric stretch observed in offline FTIR measurements that may shift part of the absorbance band outside the flow-through IR window. Intrinsic viscosity of the model LLDPEs systematically decreases with increasing branch length and is consistent across the molar mass distributions in both ambient- and high-temperature SEC. Small downturns in the intrinsic viscosity indicative of low levels of LCB are observed in the high molar mass C4 and C10 polymers due to chemical hydrogenation. Future studies will focus on higher molar mass LLDPEs to directly measure  $R_g$  and  $\varepsilon$  and determine their molar mass dependence, evaluate compactness as a function of molar mass and chain topology, and compare experimental values of  $R_g$  and  $[\eta]$  from SEC with results from molecular dynamics simulations.

The characterization of these well-controlled LLDPEs alone cannot comprehensively solve the ultimate goal of complete characterization of all mass, chemical, and topological distributions in complex mixtures of polyolefins. This work provides the first steps toward elucidating the differences in polymer architecture that can be measured with well-controlled model systems for a better understanding of structure–property relationships in polyolefin materials, which will provide useful standardized data sets. As developing commercial polymers becomes more controlled with increasing degrees of complexity, it will take a combination of the best analytical techniques with modeling and data informatics tools to provide more accurate information from analytical separation data available. In the future, a combination of computational and analytical methods will be needed to comprehensively understand convoluted polymer mixtures and ultimately develop predictive tools for designing better control of polymerizations and better methods to quantitatively characterize them.

## ■ ASSOCIATED CONTENT

### Supporting Information

The Supporting Information is available free of charge at <https://pubs.acs.org/doi/10.1021/acs.macromol.9b02623>.

NMR spectra of synthesized compounds and polymers ( $^1\text{H}$  and  $^{13}\text{C}$ ), ambient SEC chromatogram data are represented by the voltage response from differential refractive index detector, differential viscometer, and  $90^\circ$  light scattering, calibration curves for HT-SEC IR, solution FTIR spectra, and Mark–Houwink plots of polyalkenamers (PDF)

## ■ AUTHOR INFORMATION

### Corresponding Author

**Kathryn L. Beers** – Materials Science & Engineering Division, National Institute of Standards & Technology, Gaithersburg, Maryland 20899, United States; [orcid.org/0000-0003-4188-8491](https://orcid.org/0000-0003-4188-8491); Email: [kathryn.beers@nist.gov](mailto:kathryn.beers@nist.gov)

### Authors

**Sara V. Orski** – Materials Science & Engineering Division, National Institute of Standards & Technology, Gaithersburg, Maryland 20899, United States; [orcid.org/0000-0002-3455-0866](https://orcid.org/0000-0002-3455-0866)

**Luke A. Kassekert** – Department of Chemistry, University of Minnesota, Minneapolis, Minnesota 55455-0431, United States

**Wesley S. Farrell** – Materials Science & Engineering Division, National Institute of Standards & Technology, Gaithersburg, Maryland 20899, United States

**Grace A. Kenlaw** – Materials Science & Engineering Division, National Institute of Standards & Technology, Gaithersburg, Maryland 20899, United States

**Marc A. Hillmyer** – Department of Chemistry, University of Minnesota, Minneapolis, Minnesota 55455-0431, United States; [orcid.org/0000-0001-8255-3853](https://orcid.org/0000-0001-8255-3853)

Complete contact information is available at: <https://pubs.acs.org/doi/10.1021/acs.macromol.9b02623>

### Author Contributions

The manuscript was written through contributions of all authors. All authors have given approval to the final version of the manuscript.

## Notes

The authors declare no competing financial interest.

## ■ ACKNOWLEDGMENTS

The authors thank Dr. André Striegel for thoughtful discussions regarding the data and analysis.

## ■ ABBREVIATIONS

SEC, size exclusion chromatography; LLDPE, linear low-density polyethylene

## ■ ADDITIONAL NOTE

\*Official contribution of the National Institute of Standards & Technology; not subject to copyright in the United States.

## ■ REFERENCES

- (1) Sauter, D. W.; Taoufik, M.; Boisson, C. Polyolefins, a Success Story. *Polymers* **2017**, *9*, 185.
- (2) Boggioni, L.; Sidari, D.; Losio, S.; Stehling, U.; Auriemma, F.; Malafronte, A.; Di Girolamo, R.; De Rosa, C.; Tritto, I. Ethylene-Cobornene Copolymerization Using a Dual Catalyst System in the Presence of a Chain Transfer Agent. *Polymers* **2019**, *11*, 554.
- (3) Jandaghian, M. H.; Soleimannezhad, A.; Ahmadjo, S.; Mortazavi, S. M. M.; Ahmadi, M. Synthesis and Characterization of Isotactic Poly(1-Hexene)/Branched Polyethylene Multiblock Copolymer via Chain Shuttling Polymerization Technique. *Ind. Eng. Chem. Res.* **2018**, *57*, 4807–4814.
- (4) Zhang, K.; Liu, P.; Wang, W.-J.; Li, B.-G.; Liu, W.; Zhu, S. Preparation of Comb-Shaped Polyolefin Elastomers Having Ethylene/1-Octene Copolymer Backbone and Long Chain Polyethylene Branches via a Tandem Metallocene Catalyst System. *Macromolecules* **2018**, *51*, 8790–8799.
- (5) Baier, M. C.; Zuideveld, M. A.; Mecking, S. Post-Metallocenes in the Industrial Production of Polyolefins. *Angew. Chem., Int. Ed.* **2014**, *53*, 9722–9744.
- (6) Monrabal, B. Crystallization Analysis Fractionation: A New Technique for the Analysis of Branching Distribution in Polyolefins. *J. Appl. Polym. Sci.* **1994**, *52*, 491–499.
- (7) Monrabal, B.; Sancho-Tello, J.; Mayo, N.; Romero, L. Crystallization Elution Fractionation. A New Separation Process for Polyolefin Resins. *Macromol. Symp.* **2007**, *257*, 71–79.
- (8) Monrabal, B. Temperature Rising Elution Fractionation and Crystallization Analysis Fractionation. In *Encyclopedia of Analytical Chemistry*; John Wiley & Sons, Ltd.: Chichester, U.K., 2006.
- (9) Striegel, A. M.; Yau, W. W.; Kirkland, J. J.; Bly, D. D. *Modern Size-Exclusion Liquid Chromatography: Practice of Gel Permeation and Gel Filtration Chromatography*, 2nd ed.; Wiley, 2009.
- (10) Monrabal, B.; Mayo, N.; Cong, R. Crystallization Elution Fractionation and Thermal Gradient Interaction Chromatography. Techniques Comparison. *Macromol. Symp.* **2012**, *312*, 115–129.
- (11) Macko, T.; Brüll, R.; Alamo, R. G.; Thomann, Y.; Grumel, V. Separation of Propene/1-Alkene and Ethylene/1-Alkene Copolymers by High-Temperature Adsorption Liquid Chromatography. *Polymer* **2009**, *50*, 5443–5448.
- (12) Chatterjee, T.; Rickard, M. A.; Pearce, E.; Pangburn, T. O.; Li, Y.; Lyons, J. W.; Cong, R.; deGroot, A. W.; Meunier, D. M. Separating Effective High Density Polyethylene Segments from Olefin Block Copolymers Using High Temperature Liquid Chromatography with a Preloaded Discrete Adsorption Promoting Solvent Barrier. *J. Chromatogr. A* **2016**, *1465*, 107–116.
- (13) Pasch, H.; Trathnigg, B. Polyolefin Analysis by Multidimensional Liquid Chromatography. In *Multidimensional HPLC of Polymers*; Springer: Berlin, Heidelberg, 2013; pp 247–271.
- (14) Ginzburg, A.; Macko, T.; Dolle, V.; Brüll, R. Characterization of Polyolefins by Comprehensive High-Temperature Two-Dimensional Liquid Chromatography (HT 2D-LC). *Eur. Polym. J.* **2011**, *47*, 319–329.

- (15) Sun, T.; Brant, P.; Chance, R. R.; Graessley, W. W. Effect of Short Chain Branching on the Coil Dimensions of Polyolefins in Dilute Solution. *Macromolecules* **2001**, *34*, 6812–6820.
- (16) Ortín, A.; Montesinos, J.; López, E.; del Hierro, P.; Monrabal, B.; Torres-Lapasió, J. R.; García-Alvarez-Coque, M. C. Characterization of Chemical Composition along the Molar Mass Distribution in Polyolefin Copolymers by GPC Using a Modern Filter-Based IR Detector. *Macromol. Symp.* **2013**, *330*, 63–80.
- (17) Wang, W.-J.; Kharchenko, S.; Migler, K.; Zhu, S. Triple-Detector GPC Characterization and Processing Behavior of Long-Chain-Branched Polyethylene Prepared by Solution Polymerization with Constrained Geometry Catalyst. *Polymer* **2004**, *45*, 6495–6505.
- (18) Yu, Y.; DesLauriers, P. J.; Rohlfing, D. C. SEC-MALS Method for the Determination of Long-Chain Branching and Long-Chain Branching Distribution in Polyethylene. *Polymer* **2005**, *46*, 5165–5182.
- (19) Plüschke, L.; Mundil, R.; Sokolohorskyj, A.; Merna, J.; Sommer, J.-U.; Lederer, A. High Temperature Quadruple-Detector Size Exclusion Chromatography for Topological Characterization of Polyethylene. *Anal. Chem.* **2018**, *90*, 6178–6186.
- (20) Calderon, N.; Ofstead, E. A.; Judy, W. A. Ring-Opening Polymerization of Unsaturated Alicyclic Compounds. *J. Polym. Sci., Part A-1: Polym. Chem.* **1967**, *5*, 2209–2217.
- (21) Sato, H.; Okimoto, K.; Tanaka, Y. Polymerization of 5-Substituted Cyclooctenes with Tungsten and Molybdenum Catalysts. *J. Macromol. Sci., Chem.* **1977**, *11*, 767–778.
- (22) Myers, S. B.; Register, R. A. Extensibility and Recovery in a Crystalline-Rubbery-Crystalline Triblock Copolymer. *Macromolecules* **2009**, *42*, 6665–6670.
- (23) Crawford, K. E.; Sita, L. R. *De Novo* Design of a New Class of “Hard–Soft” Amorphous, Microphase-Separated, Polyolefin Block Copolymer Thermoplastic Elastomers. *ACS Macro Lett.* **2015**, *4*, 921–925.
- (24) Gianotti, G.; Dall’asta, G.; Valvassori, A.; Zamboni, V. Physical Properties of Poly-1-methyloctamer, a Model of the Ethylene/Propylene Copolymer. *Die Makromol. Chem.* **1971**, *149*, 117–125.
- (25) Lee, S. J.; McGinnis, J.; Katz, T. J. Directional Specificity and Stereoselectivity in the Metathesis of a Trisubstituted Olefin. *J. Am. Chem. Soc.* **1976**, *98*, 7818–7819.
- (26) Cho, I.; Hwang, K. M. Ring-Opening Metathesis Polymerization of 4-Methyl-6-Phenylcyclooctene. *J. Polym. Sci., Part A: Polym. Chem.* **1993**, *31*, 1079–1081.
- (27) Zhang, J.; Matta, M. E.; Hillmyer, M. A. Synthesis of Sequence-Specific Vinyl Copolymers by Regioselective ROMP of Multiply Substituted Cyclooctenes. *ACS Macro Lett.* **2012**, *1*, 1383–1387.
- (28) Kobayashi, S.; Macosko, C. W.; Hillmyer, M. A. Model Linear Low Density Polyethylenes from the ROMP of 5-Hexylcyclooct-1-ene. *Aust. J. Chem.* **2010**, *63*, 1201.
- (29) Jeong, H.; Kozera, D. J.; Schrock, R. R.; Smith, S. J.; Zhang, J.; Ren, N.; Hillmyer, M. A. Z-Selective Ring-Opening Metathesis Polymerization of 3-Substituted Cyclooctenes by Monoaryloxide Pyrrolide Imido Alkyldiene (MAP) Catalysts of Molybdenum and Tungsten. *Organometallics* **2013**, *32*, 4843–4850.
- (30) Hatjopoulos, J. D.; Register, R. A. Synthesis and Properties of Well-Defined Elastomeric Poly(Alkylbornene)s and Their Hydrogenated Derivatives. *Macromolecules* **2005**, *38*, 10320–10322.
- (31) Hayano, S.; Nakama, Y. Iso- and Syndio-Selective ROMP of Norbornene and Tetracyclododecene: Effects of Tacticity Control on the Hydrogenated Ring-Opened Poly(Cycloolefin)s. *Macromolecules* **2014**, *47*, 7797–7811.
- (32) Martinez, H.; Ren, N.; Matta, M. E.; Hillmyer, M. A. Ring-Opening Metathesis Polymerization of 8-Membered Cyclic Olefins. *Polym. Chem.* **2014**, *5*, 3507–3532.
- (33) Kobayashi, S.; Pitet, L. M.; Hillmyer, M. A. Regio- and Stereoselective Ring-Opening Metathesis Polymerization of 3-Substituted Cyclooctenes. *J. Am. Chem. Soc.* **2011**, *133*, 5794–5797.
- (34) Farrell, W. S.; Beers, K. L. Ring-Opening Metathesis Polymerization of Butyl-Substituted *Trans* -Cyclooctenes. *ACS Macro Lett.* **2017**, *6*, 791–795.
- (35) Radlauer, M. R.; Matta, M. E.; Hillmyer, M. A. Regioselective Cross Metathesis for Block and Heterotelechelic Polymer Synthesis. *Polym. Chem.* **2016**, *7*, 6269–6278.
- (36) Love, J. A.; Morgan, J. P.; Trnka, T. M.; Grubbs, R. H. A Practical and Highly Active Ruthenium-Based Catalyst That Effects the Cross Metathesis of Acrylonitrile. *Angew. Chem., Int. Ed.* **2002**, *41*, 4035–4037.
- (37) Walker, R.; Conrad, R. M.; Grubbs, R. H. The Living ROMP of *Trans*-Cyclooctene. *Macromolecules* **2009**, *42*, 599–605.
- (38) Martinez, H.; Hillmyer, M. A. Carboxy-Telechelic Polyolefins in Cross-Linked Elastomers. *Macromolecules* **2014**, *47*, 479–485.
- (39) Zimm, B. H. Apparatus and Methods for Measurement and Interpretation of the Angular Variation of Light Scattering; Preliminary Results on Polystyrene Solutions. *J. Chem. Phys.* **1948**, *16*, 1099–1116.
- (40) Podzimek, S. Combination of SEC and Light Scattering. In *Light Scattering, Size Exclusion Chromatography and Asymmetric Flow Field Flow Fractionation*; John Wiley & Sons, Inc, 2011; pp 207–258.
- (41) Andersson, M.; Wittgren, B.; Wahlund, K. G. Accuracy in Multiangle Light Scattering Measurements for Molar Mass and Radius Estimations. Model Calculations and Experiments. *Anal. Chem.* **2003**, *75*, 4279–4291.
- (42) Frijns-Bruls, T.; Ortin, A.; Weusten, J.; Geladé, E. Studies on the Application of Filter-Based IR Detector for Polyolefin Characterization with HT-SEC. *Macromol. Symp.* **2015**, *356*, 87–94.
- (43) Frijns-Bruls, T.; Ortin, A.; Weusten, J.; Geladé, E. Studies on the Use of Filter-Based IR Detector for Short-Chain Branching Characterization of Polyolefin Copolymers with High Temperature Size Exclusion Chromatography. *Polymer* **2019**, No. 121600.
- (44) De Gennes, P. G. *Scaling Concepts in Polymer Physics*; Cornell University Press: Ithaca, NY, 1979, p 324.
- (45) Striegel, A. M. Mid-Chain Grafting in PVB-Graft-PVB. *Polym. Int.* **2004**, *53*, 1806–1812.
- (46) Lusignan, C. P.; Mourey, T. H.; Wilson, J. C.; Colby, R. H. Viscoelasticity of Randomly Branched Polymers in the Vulcanization Class. *Phys. Rev. E* **1999**, *60*, S657–S669.
- (47) Podzimek, S. *Light Scattering, Size Exclusion Chromatography and Asymmetric Flow Field Flow Fractionation: Powerful Tools for the Characterization of Polymers, Proteins and Nanoparticles*; John Wiley and Sons: Hoboken, NJ, 2011.
- (48) Zimm, B. H.; Stockmayer, W. H. The Dimensions of Chain Molecules Containing Branches and Rings. *J. Chem. Phys.* **1949**, *17*, 1301–1314.
- (49) Striegel, A. M. Multiple Detection in Size-Exclusion Chromatography of Macromolecules. *Anal. Chem.* **2005**, *77*, 104 A–113 A.
- (50) Dockhorn, R.; Plüschke, L.; Geisler, M.; Zessin, J.; Lindner, P.; Mundil, R.; Merna, J.; Sommer, J. U.; Lederer, A. Polyolefins Formed by Chain Walking Catalysis—A Matter of Branching Density Only? *J. Am. Chem. Soc.* **2019**, *141*, 15586–15596.
- (51) Ostlund, S. G.; Striegel, A. M. Ultrasonic Degradation of Poly( $\gamma$ -Benzyl-L-Glutamate), an Archetypal Highly Extended Polymer. *Polym. Degrad. Stab.* **2008**, *93*, 1510–1514.